Finite Element Analysis of Nonlinear Contact Problems with Mixed Eulerian-Lagrangian Description

Binsar H. Hariandja*

Department of Civil Engineering, President University, Cikarang, Indonesia

Received 06 May 2023; received in revised form 29 June 2023; accepted 30 June 2023

Abstract

This study deals with analysis of structures using mixed Eulerian-Lagrangian description. Apart from generally used Lagrangian description which uses initial configuration as reference, the newly proposed uses one of actual configuration as reference. Therefore, the total displacement is decomposed into two portions, i.e., the portion covering displacement from initial into referential configuration called Eulerian displacement, and the portion covering displacement from referential configuration into current configuration called Lagrangian displacement. The new technique is suitable to be applied to several classes of structures such as frictional contact and tensile structures. Eulerian displacement is used to represent relative displacements between material points paired in a nodal point in which slip mode occurs, while Lagrangian displacement is used to represent mutual displacement of material points paired in a nodal point in which stick mode occurs. The method was applied to certain contact problems, and the results obtained agreed fairly well with existing results found in references.

Keywords: Mixed Eulerian-Lagrangian description, contact, friction, Coulomb

1. Introduction

Structural analysis is carried out by describing physical process with respect to a chosen referential configuration. The referential configuration chosen may be undeformed configuration or deformed configuration. In infinitesimal displacement, the undeformed configuration is usually chosen as reference, even though deformed configuration may be chosen as reference. The difference would be negligible since undeformed and deformed configurations differ only to an infinitesimal degree. As an example, if a bar with length 100 cm is stretched so as to elongate 1 cm, then the strain is 1 cm / 100 cm = 0.0100 if undeformed configuration is used as reference, and the strain is 1 cm / 101 cm = 0.0099 if deformed configuration is used as reference. But if the elongation is 50 cm, then the strain is 50 cm / 100 cm = 0.5000 if undeformed configuration is used as reference, and the strain is 50 cm / 150 cm = 0.3333 if deformed configuration is used as reference.

This concludes that for finitesimal displacement, the strain would be different if different description is used, even though the two strains describe the same deformation. The one that uses undeformed configuration as reference is referred to as Lagrangian description, and the one that uses deformed configuration as reference is referred to as Eularian description. An approach that uses a special configuration as reference called mixed Lagrangian-Eulerian description is proposed in this study, along with its examples of application.

2. The Mixed Eulerian–Lagrangian Description

Due to external loads (body force and surface traction) a system initially assumed undeformed configuration denoted as

* Corresponding author. E-mail address: binsar_hariandja@president.ac.id
Tel.: +62(0)21 89109763

V^t eventually assumed current configuration v^t as shown in Fig. 1. A special configuration is chosen to be reference. At any time t a location $\underline{x}^r$ is associated with a single particle identified by its position vectors $\underline{X}^t$ and $\underline{x}^t$. in this model, $\underline{X}^t$ and $\underline{x}^t$ are functions of time and $\underline{x}^r$, the only independent spatial variable. Assume that one-to-one mappings exist such that

$$\underline{X}^t = \underline{X}(\underline{x}^r, t)., \underline{x}^t = \underline{x}(\underline{x}^r, t) \tag{1}$$

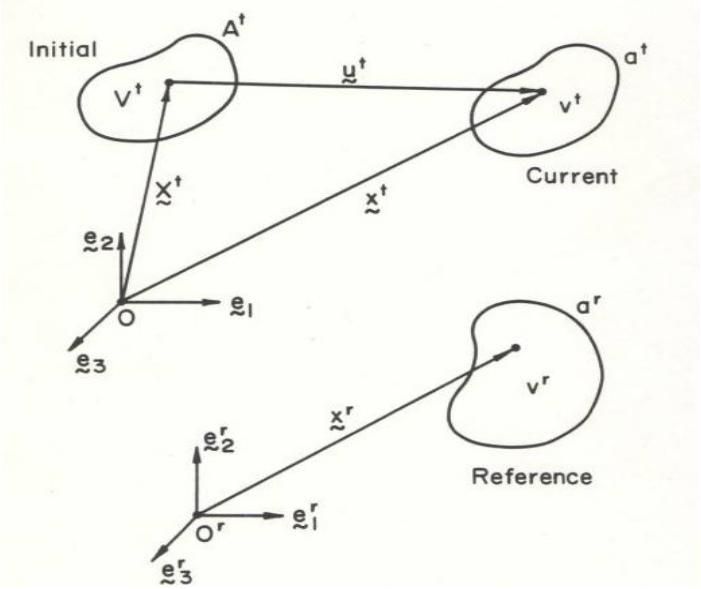

Fig. 1. Eulerian-Lagrangian kinematic model

The associated displacement vector is

$$\underline{u}^t = \underline{u}(\underline{x}^r, t = \underline{x}^t - \underline{X}^t \tag{2}$$

The components of the Green strain tensor corresponding to the total deformation are defined by

$$E_{ij} = \frac{1}{2}(J_{ki}J_{kj} - \delta_{ij}) \tag{3}$$

in which $J_{ij} = \partial x_i / \partial x_j$ are Jacobian components of the total deformation. It is convenient to decompose J_{ij} into Lagrangian and Eulerian parts, $\hat{J}_{ik}$ and $\bar{J}_{ik}$ such that

$$J_{ij} = \hat{J}_{ik}\bar{J}_{kj} \tag{4}$$

in which

$$\hat{J}_{ik} = \frac{\partial x_i}{\partial x_k^r} \; ; \; \bar{J}_{kj} = \frac{\partial x_k^r}{\partial X_j} = (\bar{J}_{kj})^{-1} \tag{5}$$

If $\bar{J}_{ij}$ is constant in time, the conventional Lagrangian description is obtained. A pure Eulerian formulation results if $\hat{J}_{ik}$ is constant in time.

To formulate equilibrium condition, an admissible virtual field denoted by $\delta\underline{u}$ is imposed on the current configuration. The principle of virtual displacement requires that

$$\int_{v^t} \tau_{ij}^t \frac{\partial \delta u_i}{\partial x_j^t} dv^t = \int_{v^t} \partial u_k \rho^t b_k^t dv^t + \int_{a_p^t} \partial u_k \rho_k^t da^t \tag{6}$$

The virtual work expression in the reference configuration is

$$\int_{v^r} W_2^t dv^r = \int_{v^r} \partial u_k \rho^0 b_k^t \bar{J}^t dv^r + \int_{a_p^r} \partial u_k \rho_k^t \, (\kappa^a)^t da^r \tag{7}$$

where W_2^t is the virtual strain energy density measured in the reference configuration and is given by

$$W_2^t = \delta u_{i,s} \bar{\bar{J}}_{sl}^t J_{ik}^t S_{kl}^t \bar{J}^t \tag{8}$$

in which the comma between subscripts denotes differentiation with respect to the reference coordinates. The stiffness equations obtained from Eq. (6) are generally nonlinear the incremental formulations which are used to derive linearized stiffness equation are given in the following discussion.

3. Incremental Formulations

An incremental model of the Eulerian-Lagrangian descriptions (ELD) is depicted in Fig. 2. The positions of the material pasticles associated with a specific references location $\underline{x}^r$ at time $t + \Delta t$ are given by

$$\underline{X}^{t+\Delta t} = \underline{X}^t + \Delta \underline{X}(\underline{x}^r, \Delta t) \; ; \; \underline{x}^{t+\Delta t} = \underline{x}^t + \Delta \underline{x}(x^r, \Delta t) \tag{9}$$

The increments $\Delta \underline{X}$ and $\Delta \underline{x}$ are treated as generalized displacements. The concept of Eulerian and Langrangian displacement components $\overline{\underline{u}}$ and $\underline{\hat{u}}$ is introduced,

$$\overline{\underline{u}} = -\Delta \underline{X} \; ; \; \underline{\hat{u}} = \Delta \underline{x} \tag{10}$$

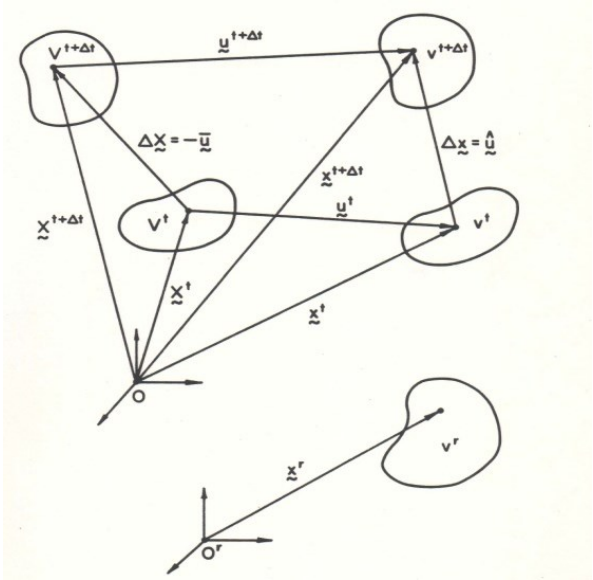

Fig. 2. Incremental deformation model

such that the total incremental displacement vector is

$$\Delta \underline{u} = \Delta \underline{x} - \Delta \underline{X} = \underline{\hat{u}} + \overline{\underline{u}} \tag{11}$$

The incremental displacements produce corresponding changes in the Jacobian, strain and stress components. After truncating terms that are quadratic in the incremental displacements, a linearized equilibrium condition in the following form is obtained.

$$\int_{v^r} [W_2^t + \Delta^L W_2] dv^r = \int_{v^r} \partial u_k \rho^0 b_k^{t+\Delta t} \, [\bar{J}^t + \Delta^L \bar{J}] dv^r + \int_{a_p^r} \partial u_k \rho_k^{t+\Delta t} \, [(\kappa^a)^t + \Delta^l (\kappa^a)] da^r \tag{12}$$

A complete derivation of the incremental formulation of mixed Eulerian-Lagrangian description may be found elsewhere [1].

4. Incremental Formulations in Finite Element

A useful form of the Eulerian-Langrarian description based on isoparametric finite element model is shown in Fig. 3 [1]. The parent element geometry is selected as the reference configuration for each element, and the element natural coordinate system is chosen to be the reference coordinate system. This requires that the reference configuration and coordinate system be defined independently for each element. The initial and current configuration coordinate and the incremental and isoparametric element are then given by

$$X_i^t = h_\alpha X_{i\alpha}^t \; ; \; x_i^t = h_\alpha x_{i\alpha}^t \; ; \; \Delta X_i = h_\alpha \Delta X_{i\alpha} \; ; \; \Delta x_i = h_\alpha \Delta x_{i\alpha} \; ; \; \delta u_i = h_\alpha \delta u_{i\alpha} \tag{13}$$

in which $h_\alpha(\underset{\sim}{x}^r)$ is the shape function associated with node α. The system of equilibrium equations given by Eq. (12) are written in partitioned form as follows.

$$[K_{\delta x} \quad K_{\delta X}] \begin{Bmatrix} \Delta x \\ \Delta X \end{Bmatrix} = \{\Delta R_x\} \tag{14}$$

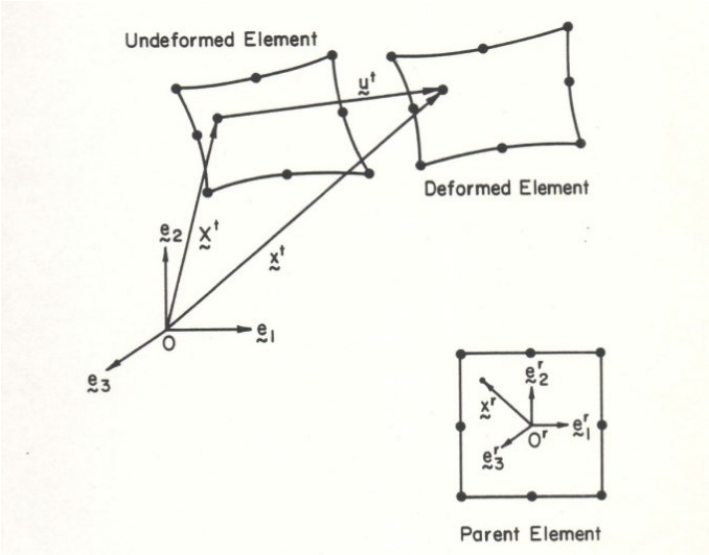

Fig. 3. Isoparametric element model of ELD

5. Examples of Applications

The Eulerian-Langrarian description may be applied to several engineering problems. In this case, the description is applied to contact problems shown in Fig. 4. Several methods for modelling contact problems are available, such as the use of constraint function as suggested by Bathe and Bouzinov [2]. The use of Eulerian-Lagrangian displacement in modelling found its interesting application to contact problems since the slip mode may be modeled by the use of Eulerian displacement part. The model used herein is the model suggested by Coulomb [3]. Incremental contact problem is depicted in Fig. 4, and the use of mixed Eulerian-Lagrangian displacement model is depicted in Fig. 5.

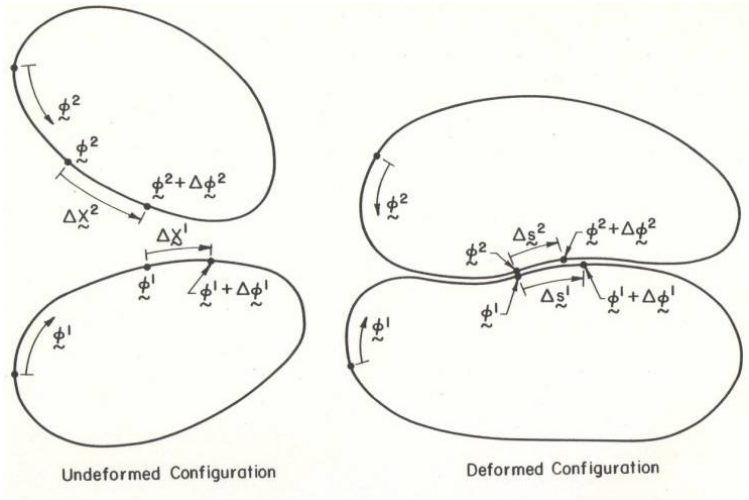

Fig. 4. Incremental Eulerian model on the contact surfaces

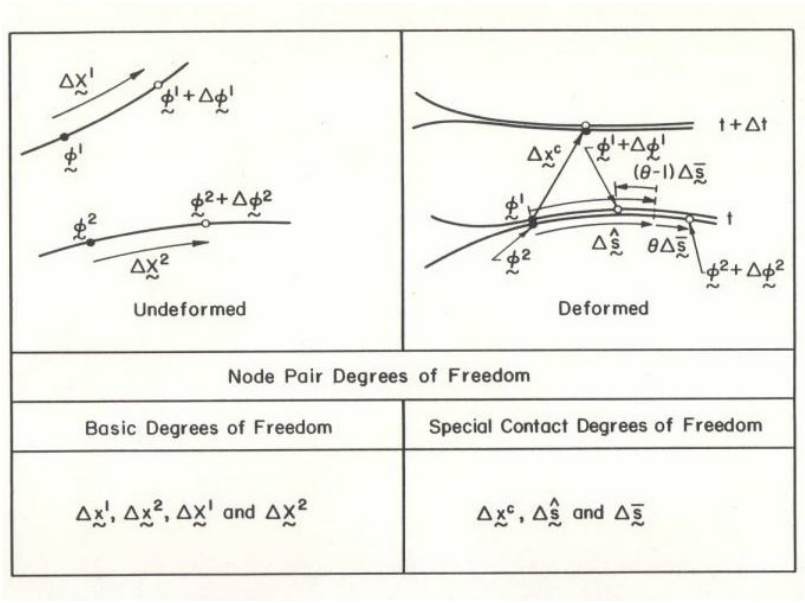

Fig. 5 Kinematic model for a contact node pair

Consider a contact problem between two bodies, in which there exist normal contact stress denoted by p_n and tangential stress p_t. Depending on the values of contact stresses, there may exist three kinds of contact mode, i.e., separation, slip and stick modest. In separation mode, the stresses are

$$p_n = 0\,; \quad p_t = 0 \tag{15}$$

whereas in stick mode,

$$p_n < 0\,; \quad \|p_t\| \le f\,; \quad and\ \dot{\underline{u}}_n = \dot{\underline{u}}_t = 0 \tag{16}$$

in which f is the allowable friction stress at contact surface, $\dot{\underline{u}}_n$ and $\dot{\underline{u}}_t$ represent relative velocity between contacting bodies in normal and tangential directions. In slip mode, it has

$$p_n < 0\,; \quad \underline{p}_t = -f\frac{\dot{\underline{u}}_t}{\|\dot{\underline{u}}_t\|}; \quad and\ \dot{\underline{u}}_n = 0 \tag{17}$$

Algorithm in the analysis of contact problem is shown in Fig. 6. The chains in contact mode is depicted in Fig. 7. In the following, several examples are presented, i.e., an elastic layer resting on a rigid foundation and an elastic resting on a rigid foundation subjected to a cyclic line load. The analysis may be cast in finite element formulation as done by Hirai et al [4].

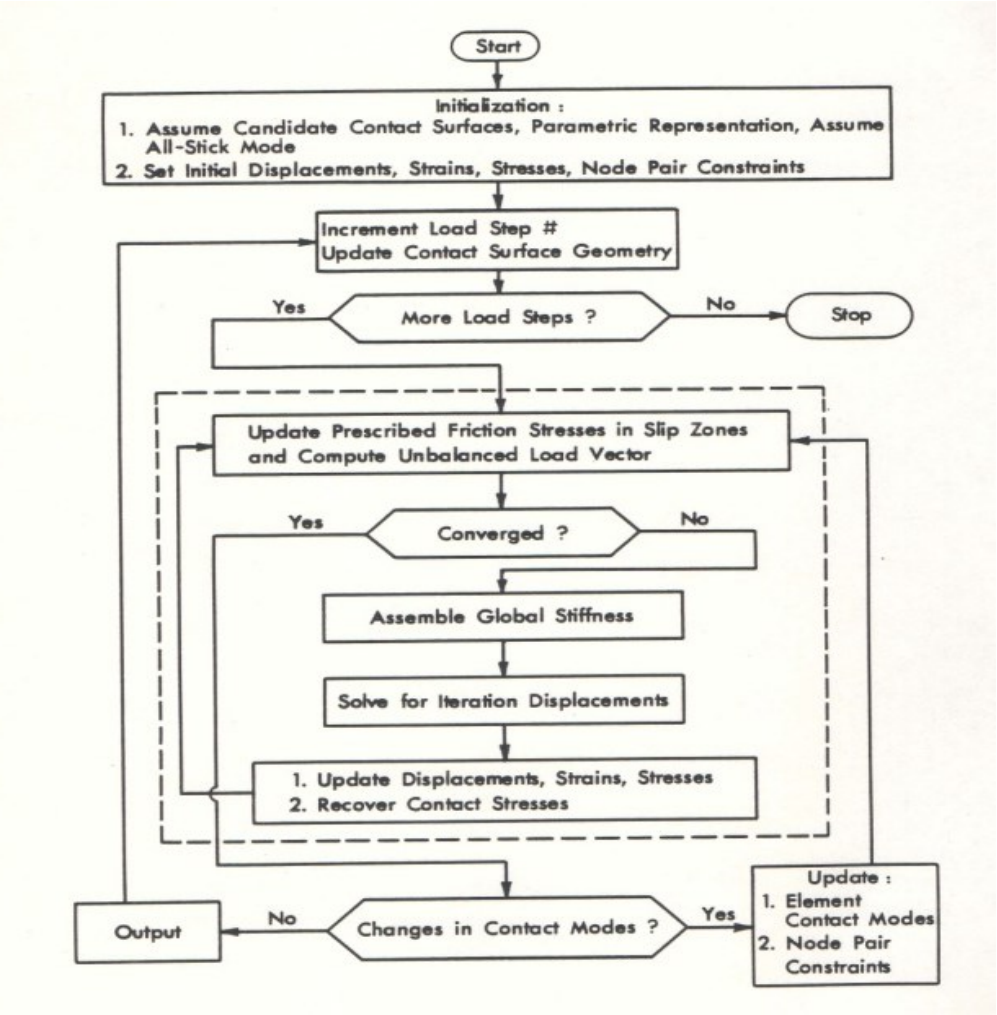

Fig. 6 Flow chart of frictional contact algorithm

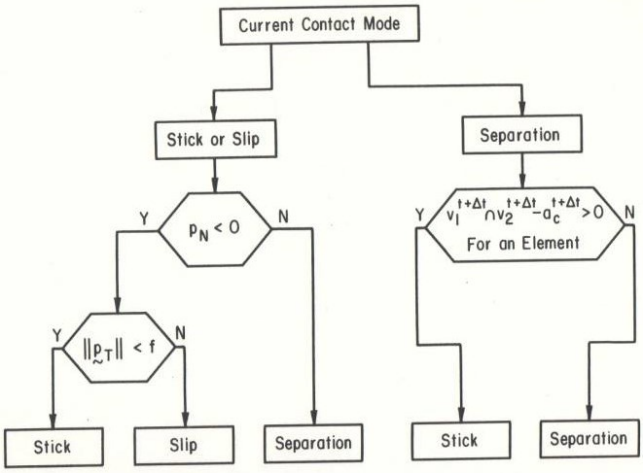

Fig. 7 Decision chart for updating element contact modes

2.1 An elastic layer resting on a rigid foundation.

A plane strain contact problem involving an elastic plate and a rigid foundation is depicted in Fig. 8. This problem was investigated previously by Civelek and Erdogan [5] and Gecit [6]. The plate is subjected to a downward distributed load denoted by p_0 and a line load $P = \lambda p_0 h$. In this analysis, proportional loading case is assumed. Due to symmetry and the local influence of the line load on the structure, only the portion of the structure shown in Fig. 8 is considered. The entire initial contact surface between the plate and the foundation is used as the candidate contact surface.

Both frictionless and frictional cases are considered. Normalized contact stress distributions for the frictionless case with several values of λ are shown in Fig. 9. In each case a separate analysis was performed and the full load was applied in a single step. Contact a long the entire candidate surface is predicted for lower values of λ. A separation region starts to develop below the line load at $\lambda = 1.088$. The determination of the contact zone topology requires relatively few iterations. The precise locations of the transition contours are determined using a small number of additional iterations. as an example, for $\lambda = 2.0$, the analysis requires four iterations to determine the contact zone topology and seven iteration to adaptively locate the precise transition locations.

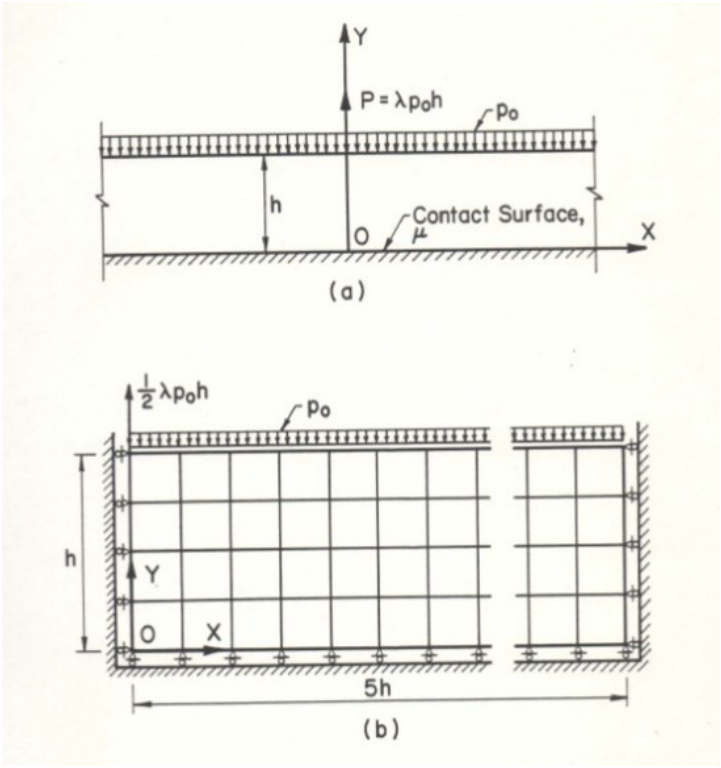

Fig. 8 An elastic plate resting on a rigid foundation

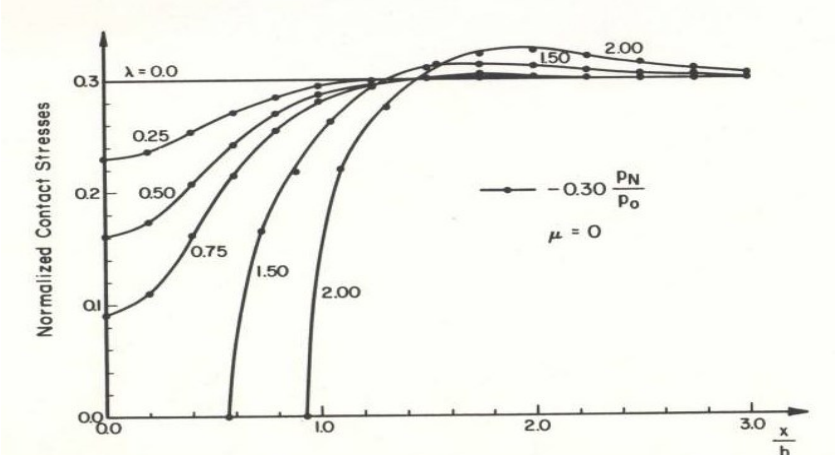

Fig. 9 Normalized contact stressess, frictionless case

Next, frictional case is considered. The normalized contact stress distribution are shown in Fig. 10. For larger values of λ a separation zone develops below the line load. Immediatly outside the separation region is a zone of slip, and the remainder of the contact surface sticks. the frictional stresses cause bending deformations which reduce the extend of separate region. The frictional solution requires more iterations than the frictional case. For example, for $\lambda = 2.0$, the solution requires eight iterations to determine the contact zone topology, compared to four in frictionless case, and twelve iterations to precisely locate the transition contour (compared to seven iterations in the frictionless case).

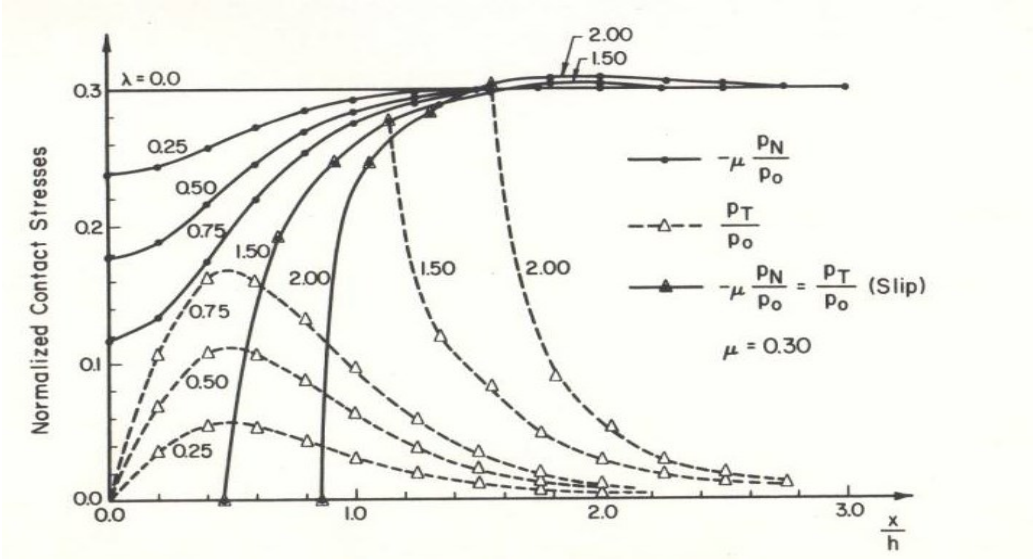

Fig. 10 Normalized contact stressess, frictional case

2.2 An elastic layer resting on a rigid foundation subjected to a cyclic line load.

The structure in the previous section is reconsidered with a cyclic variation of the line load P. An incremental version of the adaptive procedure is used to incorporate history-dependent effects. A refined finite element mesh is used in anticipation of the contact zone geometries for the loading and unloading paths. The line load P is specified by varying the parameter λ between 1.2 and 2.0 in increments of 0.10. The distributed load is held constant through the analysis. The solution in section 5.1 for $\lambda = 1.2$ is assumed as the initial condition for the analysis. The contact zone topology and the initial location of the transition contours are determined from this solution.

Normalized stress ditributions for the frictionless case and selected values of λ are shown in Fig. 11, Fig. 12 and Fig. 13. Comparizon with Fig. 8 indicates that the computed response is essentially independent of the load history, as expected for the frictional case.

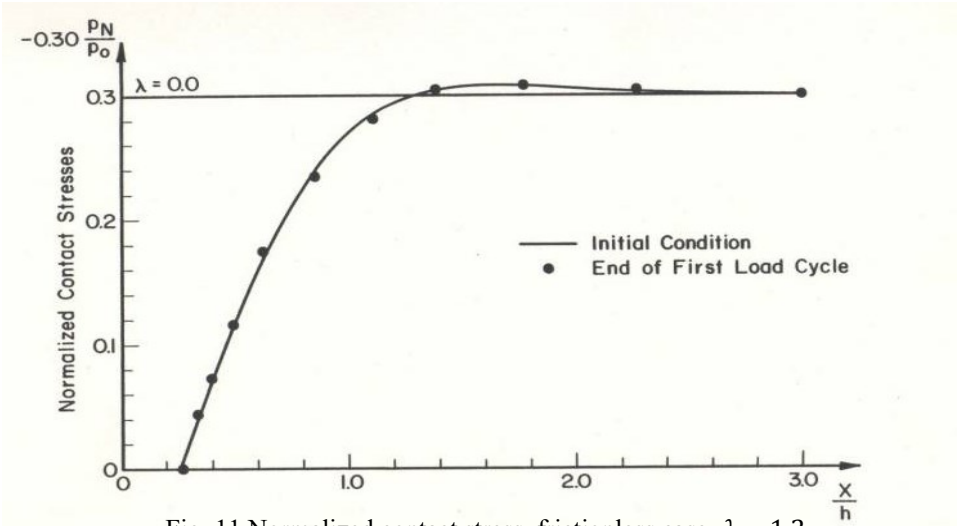

Fig. 11 Normalized contact stress, frictionless case, $\lambda = 1.2$

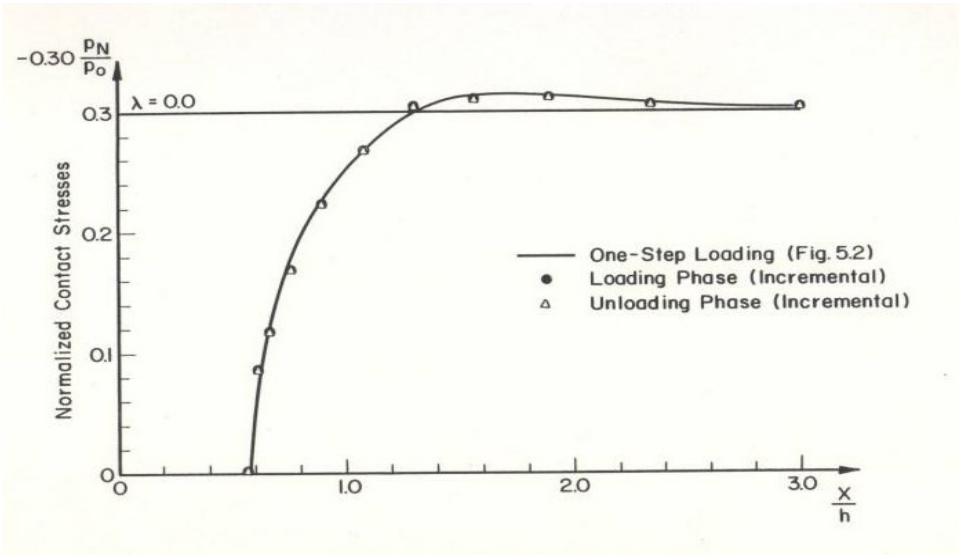

Fig. 12 Normalized contact stress, frictionless case, $\lambda = 1.5$

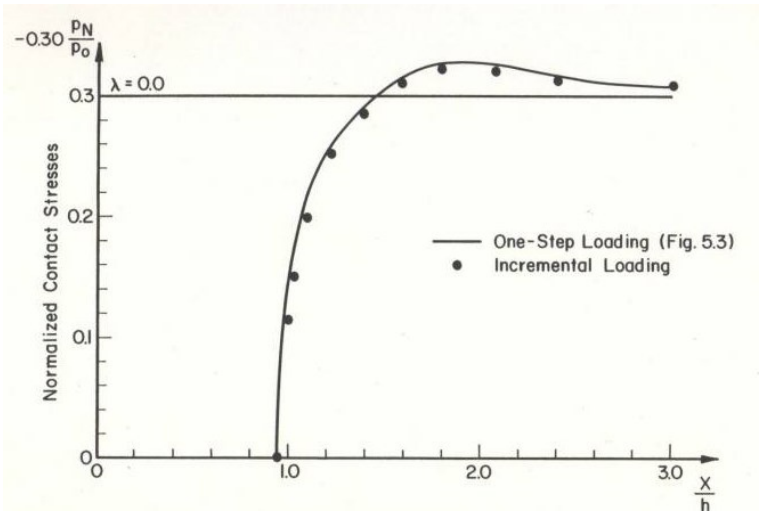

Fig. 13 Normalized contact stress, frictionless case, $\lambda = 2.0$

Normalized contact stress distribution for the frictional case are plotted in Fig. 14, Fig. 15 and Fig. 16 for $\lambda = 1.2$, $\lambda = 1.5$, and $\lambda = 2.0$, repectively. Results from Fig. 12 are also shown for comparison. The results indicated history-dependent behavior for frictional case during the loading phase, and support the generality of the solutions persented in Fig. 12. However, the structure exhibits very different behavior during the unloading phase. Immediately after the line load intensity begins to decrease, a reduced slip zone develop and the region adjacent to the separation zone. This effect can be seen in Fig. 15 where the contact stress distribution are compared for $\lambda = 1.5$ during the loading and unloading phases. Note that the slip displacements and friction stresses undergo a reversal in the loading phase. The remainder of the contact surface exhibits stick behaviour. This example clearly demonstrates that frictional contact is generally a history-dependent process.

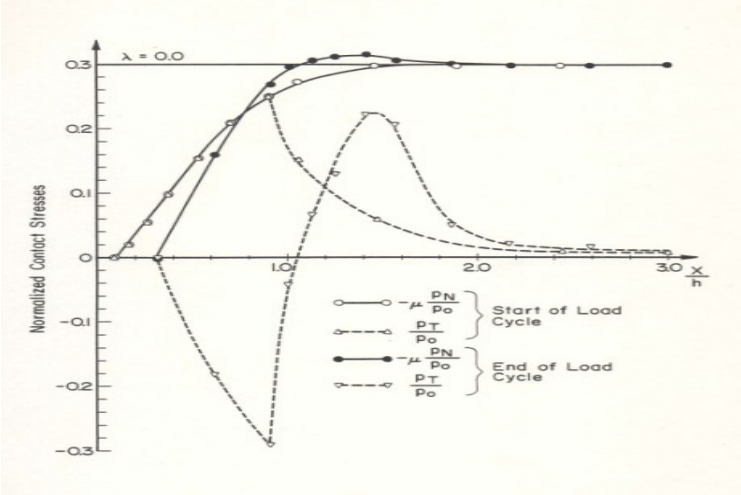

Fig. 14 Normalized contact stress, frictional case, $\lambda = 1.2$

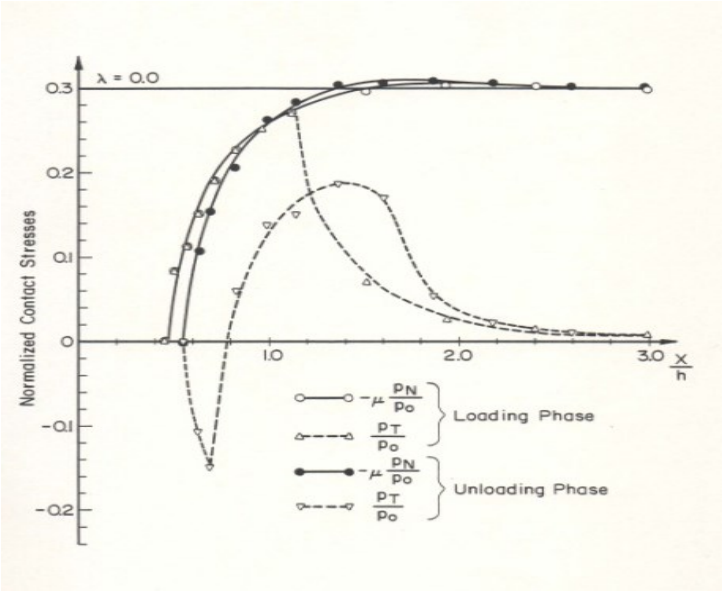

Fig. 15 Normalized contact stress, frictional case, $\lambda = 1.5$

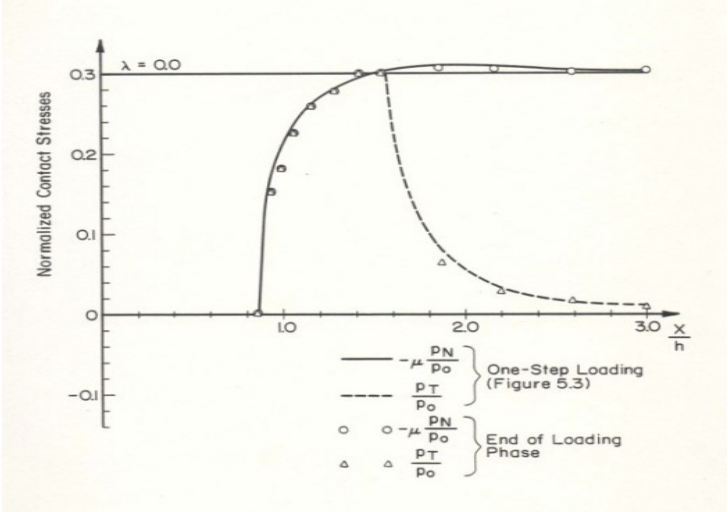

Fig. 16 Normalized contact stress, frictional case, $\lambda = 2.0$

6. Conclusions

This study has described the development of novel finite element algorithms for frictional contact problems. These algorithms make use of a new topological description of the frictional contact problem and new computational techniques for computing surface tractions and performing adaptive finite element analysis. The mixed Eulerian-Langrangian kinematic description places a central role in the contact algorithm. The effectiveness of the algorithms has been demonstrated for example problem involving the Coulomb friction law, curved contact surfaces, large deformation un-cycling loading.

A frictional contact algorithm based on a heuristic approach was presented in the study. The algorithm is capable of determining contact zone topology and geometry within the resolution of the element mesh. The effectiveness of the algorithm has been demonstrated in examples involving receding contact problem.

Acknowledgments

The writer wishes to extend his sincere gratitude to Professor Robert B. Haber for his assistantship and guidance during the writer's Doctor of Philosophy program at University of Illinois at Urbana-Champaign, USA. The writer also extends his appreciation to Mr. Muhammad Azhar Dwitama, and Mr. David Hariandja for typing the manuscript patiently and excellently.

References

[1] B. H. Hariandja, Adaptive Finite Element Analysis of Nonlinear Frictional Contact with Mixed Eulerian-Lagrangian Coordinates, Ph.D. Dissertation, Civil Engineering Department, University of Illinois at Urbana-Champaign, USA, 1985.
[2] K. J. Bathe and P. A. Bouzinov, "On the Constraint Function Method for Contact Problems," Computers and Structures, vol. 64, no. 5/6, pp. 1069-1085, 1997.
[3] C. A. Coulomb, "Theorie des Machines Simples," Memorie de l'Academie Royale A, pp. 161-342, 1785.
[4] A. Awaludin, T. Hirai, T. Hayashikawa and A. J. M. Leijten, "A Finite Element Analysis of Bearing Resistance of Timber Loaded through a Steel Plate," Civil Engineering Dimension, vol. 14, no. 1, 2012.
[5] M. B. Civelek and F. Erdogan, "The Frictionless Contact Problems for an Elastic Layer Under Gravity," Journal of Applied Mechanics, vol. 42, pp. 136-140, 1975.
[6] M.R. Gecit, "A Tensionless Contact Without Friction Between an Elastic Layer and an Elastic Foundation," International Journal of Solids and Structures, vol. 16, pp. 387-396, 1980.